Gas Separation Properties of Organosilicon Plasma Polymerized Membranes

Stéphanie Roualdes, Arie Van der Lee, René Berjoan, José Sanchez, and Jean Durand
Laboratoire des Matériaux et Procédés Membranaires (UMR 5635), ENSCM, 34296 Montpellier Cedex 5, France

Thin films were polymerized from different organosilicon compounds in a radio-frequency plasma deposition process. The properties of the layers were characterized with respect to the deposition rate, the density, the refractive index, and the chemical structure determined by FTIR and XPS analysis. The qualification of the films for gas-selective membranes was tested on different porous substrates using N_2, H_2, O_2, CO_2, and CH_4. Both structure and permeation performances of the synthesized films were correlated with the composite plasma parameter $V/F \cdot M$ (V: input voltage; F: monomer flow rate; M: monomer molecular weight). At low $V/F \cdot M$ ratio, the thin layers are mainly constituted of the $[(CH_3)_2-Si(-O)_2]$ environment (monomer and polydimethylsiloxane one). Increasing the $V/F \cdot M$ results in a more ''inorganic'' chemical structure, higher O/Si ratio, refractive index, and density, the materials tend toward a silicalike structure. Concurrently, the prepared membranes have solution–diffusion-controlled or Knudsen-like separation factors, depending on whether plasma conditions are soft or hard.

Introduction

Plasma polymerization has been recognized as a unique method for preparing uniform, pinhole-free and thin polymeric films (Bell, 1974; Yasuda, 1978; Chapman, 1980; D'Agostino, 1990). This polymerization process is a powerful technique that allows us to obtain highly cross-linked polymers from nonfunctional monomers that are not utilized in conventional polymer synthesis. The properties of the plasma polymers formed are naturally affected by the molecular structure of the original monomer as well as the operating parameters such as power input, monomer flow rate, and pressure in the reaction chamber.

Plasma polymers deposited from organosilicon precursors are promising materials for gas-separation processes. Indeed, silicon-containing polymers are well known as polymers excelling in gas permeation; when these are synthesized by the plasma process, they also exhibit high selectivities because of their high cross-linking compared with conventional polymers (Inagaki, 1993; Matsuyama et al., 1994b; Görbig et al., 1998). Now permeation properties of the prepared layers are very dependent on the more or less energetic character of the plasma. Indeed, it is possible to produce materials either mainly composed of silica or close to silicone-like polymers, depending on whether the plasma conditions are hard or soft (Yasuda, 1978). Consequently, a wide range of gas permeabilities and selectivities can be obtained according to the more or less organic character of the films.

In this study, the plasma polymers were prepared from three different organosilicon monomers: diethoxydimethylsilane (DEDMS), hexamethyldisiloxane (HMDSO), and octamethyltrisiloxane (OMTSO). Films were deposited upon silicon wafers and different porous substrates. In order to characterize the growth kinetics of our polymers, thickness measurements were performed using scanning electron microscopy (SEM). The chemical structure of SiO_xC_y:H layers was investigated using both Fourier-transform infrared spectroscopy (FTIR) and X-ray photoelectron spectroscopy (XPS) analysis. The film density and refractive index were studied using X-ray reflectometry and ellipsometry, respectively. The permeation properties of the films were determined by the pressure-increase method using N_2, O_2, H_2, CO_2, and CH_4.

Correspondence concerning this article should be addressed to J. Durand.
Present address of R. Berjoan: Institut de Science et de Génie des Matériaux et Procédés, CNRS B.P 5, Odeillo, 66125 Font-Romeu, France.

The purpose of this work is to reveal the relationship between the plasma conditions in the preparation of films (more precisely the power input, the monomer partial pressure, and the monomer molecular weight), the structure of the resulting materials, and their gas permeation performances.

Experimental Procedure

Plasma polymerization

Thin-film membranes were plasma polymerized by glow discharge at 40 kHz in a homemade capacitively coupled parallel-plate reactor (Figure 1). The system consisted of a bell-jar chamber (200 mm diameter, 200 mm high), a monomer inlet, a capacitance-diaphragm gauge (CDL 11 S12, 0–10 torr, Tylan General), a vacuum system (composed of a Trivac D 40B Leybold primary pump and a Turbovac 50 Alcatel pump), and a pair of stainless-steel parallel electrodes (140 mm diameter) separated by a distance of 50 mm. The pressure in the reactor was controlled by a throttle valve (Tylan MDV) monitored by a pressure-measure system. The substrate was horizontally placed on the lower grounded electrode, which was rotated during plasma polymerization by an electric motor drive to obtain homogeneous plasma-polymer deposition on the substrate.

The experimental procedure was as follows: the reaction chamber was evacuated down to 1.5 Pa. The vapor of the monomer (supplied by Aldrich and used without further purification) was adjusted to a fixed flow rate and injected into the reaction chamber without any carrier gas. Then, the rf (radio-frequency) power (controlled by peak-to-peak voltage value) was turned on, and glow discharge polymerization was sustained for a suitable duration. Both the rf voltage and the monomer flow rate were the operating parameters and were varied, while the pressure in the chamber was fixed at 40 Pa.

Film characterizations

The growth kinetics were studied for four different substrates: silicon wafers and three porous substrates (MF 25 Millipore made of mixed esters of cellulose, polypropylene Celgard 2400, and alumina Anodisc 47). The plasma polymers' thickness was determined from SEM pictures of the cross section of the composite membranes using a Field Emission Scanning Electron Microscope S-4500 Hitachi. The global error related to thickness measurements, including the random (or sampling) error and the error inherent in the visual evaluation of the thickness, was estimated at 10%. The analytic techniques used for film characterizations were per-

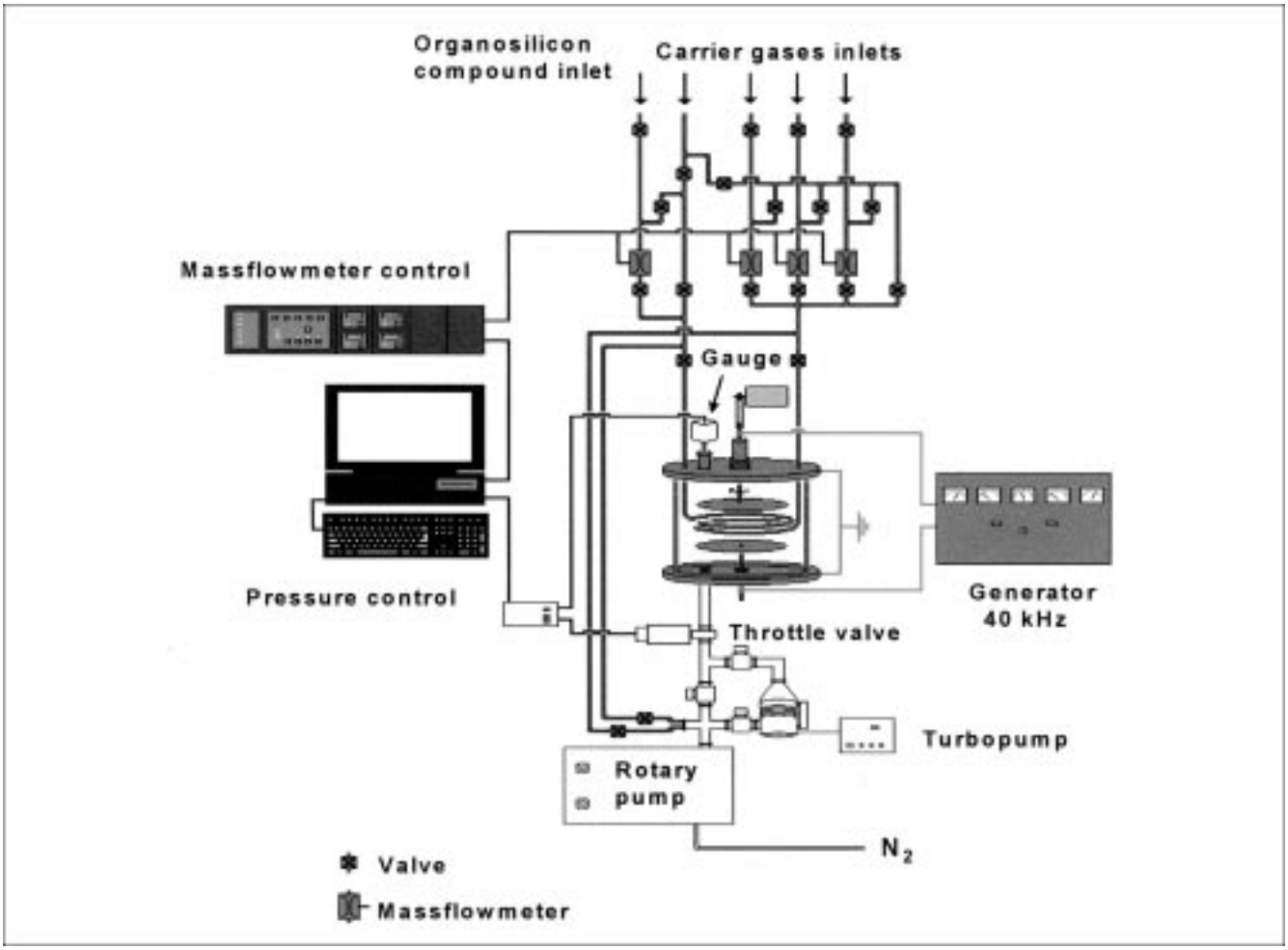

Figure 1. Plasma deposition unit.

formed using silicon wafers. FTIR absorption (using a Nicolet Impact 400D spectrometer) and XPS [using a Cameca Ribber UHV device working with a MAC2 electron spectrometer-standard compound:polydimethylsiloxane (PDMS)] were used to investigate the films' chemical structure. The XPS peaks' binding energies are given with a precision of ± 0.2 eV. The error for XPS quantitative data is estimated at 5%. XPS measurements were performed without any previous ionic bombardment in order not to destroy the real structures of the atomic layers. This leads to the risk of overestimating the oxygen and above all carbon contents. X-ray reflectometry was used to measure the film density. The experiments were performed at a wavelength of 0.154 nm with a Siemens D5000 diffractometer apparatus specially modified to work at very low angles. For a grazing angle α higher than the critical angle α_c, X-rays can penetrate into the film, thus causing the reflected intensity to suddenly decrease. An angular measurement allows us to find the averaged electron density (since α_c is proportional to the square root of the electron density) of the thin film plus that of the substrate. The thin-film electron density is obtained by the complete modeling of the reflectivity curve using Parrat's recursive calculation method for stratified media (Parrat, 1954). The measured electron density, ρ_e, is expressed in units of "mass density," ρ_m, according to the formula $\rho_e = 2K\rho_m$, where $K = \Sigma_i Z_i/\Sigma_i A_i$, Z_i being the atomic charges, and A_i the atomic masses. Since K is nearly equal to 0.5, the electron density (in "mass units") is equal to the mass density at a few percent. The accuracy of the density is estimated to ± 0.05 $g \cdot cm^{-3}$. Ellipsometry (using a Plasmos SD 2300 with a 632.8-nm-wavelength laser ellipsometer) gives access to the refractive index (precision: ± 0.02).

Gas permeation

Permeation experiments were carried out by using the constant-volume and variable-pressure technique in a permeametry apparatus at constant temperature (298 K). The apparatus consisted essentially of a two-compartment permeation cell. The permeability was obtained by measuring the pressure increase in the downstream compartment (with a constant volume of 2.9×10^{-5} m^3) and using an MKS Baratron pressure transducer (range between 0.0 and 10^3 Pa). Three different kinds of substrates were used for permeation measurements: MF 25 millipore made of mixed cellulose esters (mean pore size: 25 nm; porosity: 70%), polypropylene Celgard 2400 (mean pore size: 40 nm; porosity: 28–40%), and alumina Anodisc 47 (mean pore size: 20 nm; porosity: 60%). The supported membranes (1.6×10^{-3} m^2) were placed between the two compartments of the permeation cell. The upstream and downstream walls of the membrane were strongly outgassed *in situ* for 2 h at high vacuum (1.0×10^{-5} Pa) using a turbomolecular pump (Leybold, Turbovac 50). The permeability experiments were performed by using 3.0×10^5 Pa of upstream pressure and recording the pressure increase in the downstream compartment. The magnitude of the purity of the gases used for the permeation measurements (N_2, O_2, H_2, CO_2, and CH_4) was of 99.95%. These gases were used without any further purification.

If we know the downstream pressure increase to be a function of time (dP_2/dt), the upstream pressure (P_1), the apparatus volume (Va), and the membrane area (A) and thickness (l), the permeability coefficient P can be determined using $P = l \cdot Va \cdot (dP_2/dt)/[10^5 \cdot A \cdot (P_1 - P_2)]$ [P is expressed in $m \cdot mol\ (STP) \cdot m^{-2} \cdot s^{-1} \cdot Pa^{-1}$]. Based on these coefficients for gases A and B, the ideal separation factor α_B^A of a membrane can be determined to be $\alpha_B^A = P_A/P_B$.

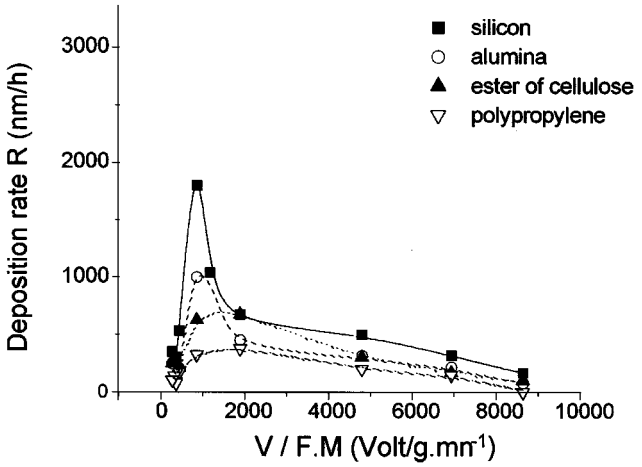

Figure 2. Deposition rate of PP-HMDSO vs. $V/F \cdot M$.

Results and Discussion

Film growth

Figures 2 and 3 show the evolution of PP-HMDSO and PP-OMTSO deposition rates (R) as a function of the $V/F \cdot M$ value (V: input voltage; F: monomer flow rate; M: monomer molecular weight). V was maintained constant equal to 50 V, and F was varied. Whatever the nature of the monomer, two regions can be distinguished: for $V/F \cdot M > 800$ $V/g \cdot min^{-1}$, we see that R decreases (first rapidly, and then slower) when $V/F \cdot M$ increases, that is, when F decreases; in this region (F low or medium), the deposition rate is limited by the amount of monomer in the gas phase. For $V/F \cdot M < 800$ $V/g \cdot min^{-1}$ (the limit at which R reaches a maximum), the growth kinetics decrease suddenly when F increases: this saturation

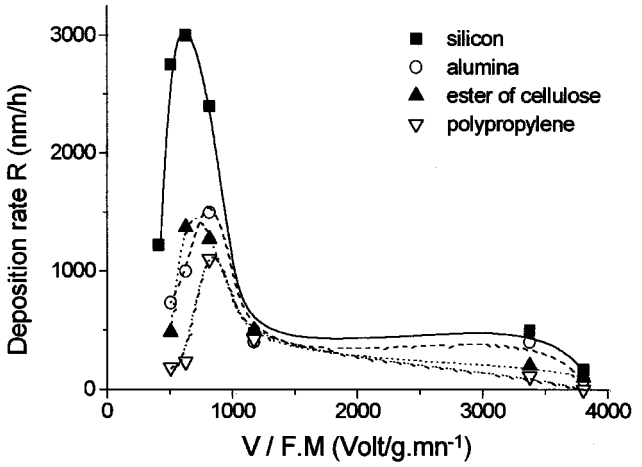

Figure 3. Deposition rate of PP-OMTSO vs. $V/F \cdot M$.

phenomenon is characteristic of the power-deficient region (Catherine and Zamouche, 1985). Both figures also show the influence of the substrate nature on the films' deposition rate. We can see that R is very dependent on the surface state (porosity, roughness, and surface-free energy) of porous substrates; it appears that the more hydrophobic the substrate, the more difficult growth is (the most important differences appear near the saturation region for a high R value) (Inagaki, 1996). The same evolution has already been shown for PP-DEDMS (Roualdes et al., 1998). Finally, we can observe that, for the same $V/F \cdot M$ value, OMTSO, which has the longest siloxane chain, gives rise to deposition rates that are twice as fast as those induced by HMDSO, because the deposited unit structure is larger (Matsuyama et al., 1994a).

Film composition

FTIR Analysis. Figure 4 shows the FTIR spectra of three PP-DEDMS deposits synthesized in different plasma conditions: very soft (high monomer flow rate and low power unit), very hard (low monomer flow rate and high power input), and medium conditions. The parameter W/FM, first presented by Yasuda (Yasuda, 1978) to describe the characteristics of the plasma polymerization, denotes an input energy per unit mass of monomer. The ratio $V/F \cdot M$ proportional to W/FM, is the parameter we introduce to describe the energetic character of the plasma polymerization. The films studied are characterized by $V/F \cdot M$ values that are equal to 693 V/g·min^{-1}, 5,484 V/g·min^{-1}, and 13,268 V/g·min^{-1} from the softest to the hardest plasma conditions. In spectra related to both films that have the lowest $V/F \cdot M$ values there are major absorbances in the 2,960–2,850-cm^{-1} region related to hydrocarbon groups (and above all at 2,960 cm^{-1}: CH_3 stretching), at 2,250–2,150 cm^{-1} (Si–H_2 and Si–H stretching), 1,260 cm^{-1} (Si–CH_3 deformation), 1,100–1,000 cm^{-1} (1,060 cm^{-1}: Si–O–Si stretching and 1,020 cm^{-1}: Si–O–R stretching), 885 and 800 cm^{-1} (Si–$(CH_3)_2$ rocking), and 850 cm^{-1} (Si–$(CH_3)_3$ rocking) (Anderson, 1974; Smith, 1977). The Si–H and Si–H_2 groups in the plasma polymers, which are not contained in the monomer, were formed by the dissociation of the Si–CH_3 and Si–O groups (Lee and Lee, 1998). The polymer deposited during the softest conditions ($V/F \cdot M = 693$ V/g·min^{-1}) is characterized by two other bands at 1,410 cm^{-1} (CH_3 deformation) and 960 cm^{-1} (Si–CH_3 rocking). On a spectrum corresponding to the hardest conditions ($V/F \cdot M = 13{,}268$ V/g·min^{-1}), only the bands related to the Si–O–Si bonds appear (stretching at 1,100–1,000 cm^{-1}, deformation at 845 cm^{-1}, and rocking at 450 cm^{-1}); this spectrum is very close to that for SiO_2.

More generally, we observe a decrease in absorptions related to "organic" groups (above all at 2,960, 1,260, and 800 cm^{-1}) when $V/F \cdot M$ increases. This suggests that the monomer structure is better preserved and the plasma polymers formed are more "polymerized" under soft conditions. The higher the $V/F \cdot M$ value, the more inorganic and crosslinked the films are.

The nature of the monomer also has influence on the chemical composition of the synthesized materials. Figure 5 shows the FTIR spectra of plasma polymers deposited under the same conditions (softest ones) from the three different precursors. We can observe that the contribution of "organic" bounds (in particular CH_3 stretching at 2,960 cm^{-1} and Si–CH_3 at 1,260 cm^{-1}) with respect to the "inorganic" ones is all the more important when the monomer siloxane chain is longer, probably because the monomer structure is better preserved (Matsuyama et al., 1994a).

In order to account for the more or less organic character of these mixed materials, we introduce the arbitrary parameter T, called the "polymerization ratio," which is equal to the ratio of the intensity of the peak at 1,260 cm^{-1} (Si–CH_3 bonds representative of the organic groups) to the intensity of the peak at 1,100–1,000 cm^{-1} (Si–O–Si and Si–O–R bonds representative of the inorganic groups). In Figure 6, T is plotted as a function of $V/F \cdot M$. Except in the saturation region ($V/F \cdot M < 800$ V/g·min^{-1}), where the tendency is reversal, T decreases from a maximum value (for the more organic and polymerized film deposited under the softest conditions) to 0 (film close to silica) when $V/F \cdot M$ increases. The maximum value of T (0.84 for PP-OMTSO, 0.65 for PP-HMDSO, and 0.43 for PP-DEDMS) is that much higher because the

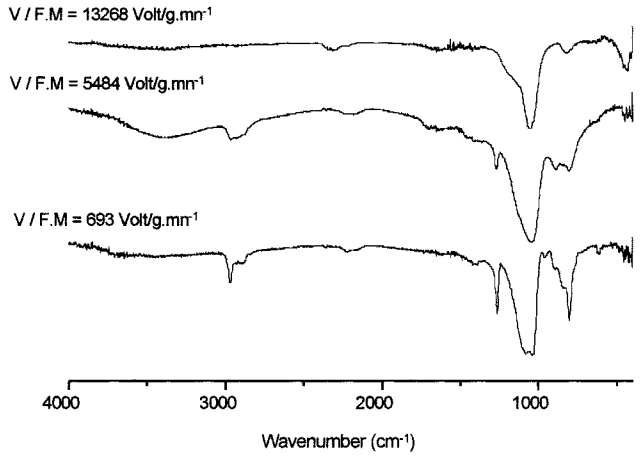

Figure 4. FTIR spectra of PP-DEDMS deposited in different plasma conditions.

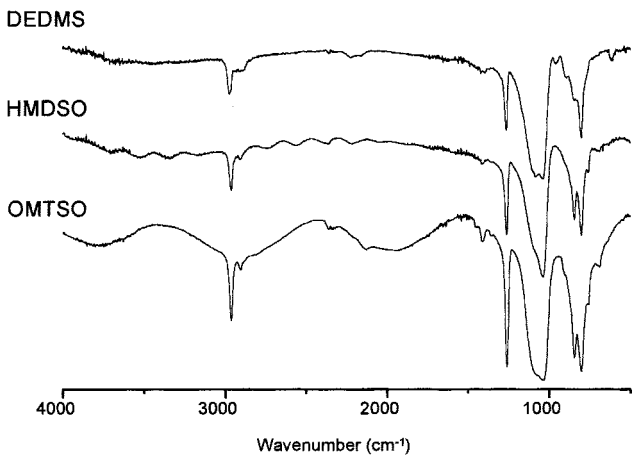

Figure 5. FTIR spectra of plasma polymers deposited in soft conditions.

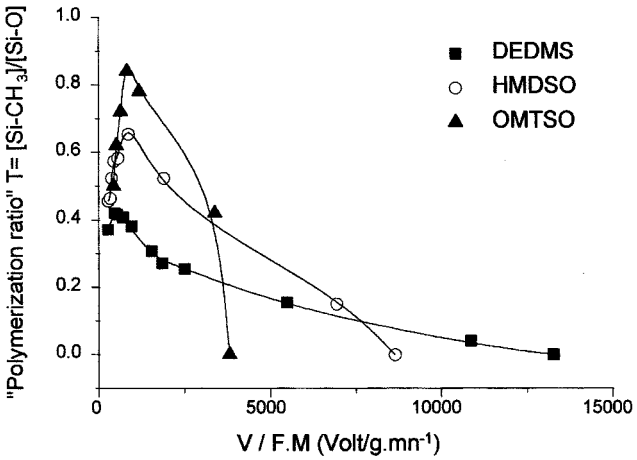

Figure 6. Evolution of the polymerization rate *T* vs. *V/F · M*.

monomer siloxane chain is longer. Moreover, the larger the precursor is, the faster T decreases when $V/F \cdot M$ is increasing.

XPS Analysis. Core-line binding energies are indicative of the chemical environment of the atom from which the electrons were emitted. Core-line widths may be used to provide a qualitative measure of the diverse states within any one peak. Table 1 shows the change in the core-line binding energies of Si_{2p} in PP-DEDMS and PP-HMDSO resulting from an increase in $V/F \cdot M$. Whatever the monomer is, most of the films synthesized in the softest conditions are mainly composed of the SiO_2C_2 environment (PDMS one), and are very polymerized. As $V/F \cdot M$ increases, the contributions of the SiC_4 (99.5-eV), $SiOC_3$ (100.8-eV), and above all SiO_2C_2 (101.9-eV) environments decrease, whereas the SiO_3C (102.8-eV) and SiO_4 (103.6-eV) peak areas increase. This shows the reduction of the organic and polymeric character of the structure. Under very hard conditions, the contribution of the $SiOC_3$ and above all SiC_4 environments is negligible; the PP-DEDMS film deposited at $V/F \cdot M = 13{,}268$ V/g·min^{-1} is composed principally of SiO_4 (48%).

Table 2 shows the change in the core-line binding energies of C_{1s} in PP-DEDMS and PP-HMDSO that result from an increase in $V/F \cdot M$. Whatever the monomer is, the plasma polymers deposited in soft and medium conditions have similar compositions. They are composed principally of an $SiCH_3$ environment (at 284.6 eV), which is characteristic of the corresponding conventional polymer PDMS. The other environments present in these films are C-O (286.3 eV) and to a

Table 1. Relative Proportions of Si Environments in PP-DEDMS and PP-HMDSO from Si_{2p} XPS Analysis

Monomer Nature	DEDMS			HMDSO		
$V/F \cdot M$ (V·min·g^{-1})	525	1841	13268	436	1891	6934
SiO_4 (103.6 eV)	5%	9%	48%	8%	8%	17%
SiO_3C (102.8 eV)	27%	29%	40%	14%	19%	37%
SiO_2C_2 (101.9 eV)	57%	51%	12%	52%	52%	39%
$SiOC_3$ (100.8 eV)	9%	7%	0%	22%	18%	7%
SiC_4 (99.5 eV)	2%	4%	0%	4%	3%	0%

Table 2. Relative Proportions of C Environments in PP-DEDMS and PP-HMDSO from C_{1s} XPS Analysis

Monomer Nature	DEDMS			HMDSO		
$V/F \cdot M$ (V·min·g^{-1})	525	1841	13268	436	1891	6934
C = 0 (288.3 eV)	0%	0%	14%	0%	0%	5%
C−O (286.3 eV) (−C−O−C or Si−O−C)	25%	24%	28%	13%	13%	24%
Si−CH_3 (284.6 eV)	65%	62%	49%	84%	81%	62%
C bonded to 2 or 3 Si (283.5 eV)	10%	14%	9%	3%	6%	9%

lesser extent C bonded to two or three Si molecules (283.5 eV). The plasma polymers deposited under the hardest conditions contain a supplementary carbon environment attributed to R−C(−O) = 0 at 288.3 eV (Wagner et al., 1978). These results also show the effect of the siloxane chain length on the films' chemical composition. Indeed, HMDSO, which has the longest chain, can form polymers containing 84% $SiCH_3$ groups; the most polymerized PP-DEDMS films contain only 65% such groups.

The Si, C, or O concentrations in the films can be determined by measurements of the Si_{2p}, C_{1s}, or O_{1s} core-level peak areas. The carbon or oxygen content of the films represented by the carbon- or oxygen-to-silicon ratios, respectively, are plotted against $V/F \cdot M$ in Figure 7. For low $V/F \cdot M$ values, the films' composition is similar to that of PDMS $[SiO(CH_3)_2]_n$, and above all for the PP-OMTSO layers (C/Si = 2.04, O/Si = 0.96) synthesized from the monomer with the longest siloxane chain. Parallel to the increase in the inorganic character in polymers shown by FTIR analysis, O/Si logically increases with increasing $V/F \cdot M$. This is due to the increase in residual radicals that can react with oxygen or water vapor in the atmosphere when the plasma conditions become harder. C/Si decreases with $V/F \cdot M$ because the more reactive silicon-containing fragments contribute to a larger extent to the deposition (Matsuyama, 1994c). At the greatest $V/F \cdot M$ condition, the film composition can be attributed to silicon polluted by carbon (O/Si is close to 2 for all polymers).

The XPS results confirm the chemical composition shown by the FTIR spectra. Both analyses show that it is possible to

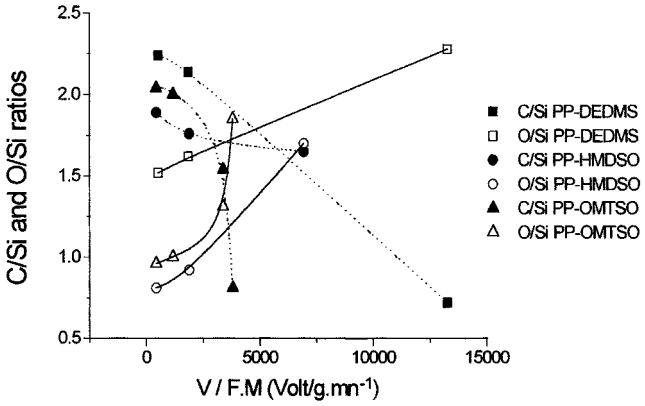

Figure 7. Evolution of O/Si and C/Si ratios as a function of *V/F · M*.

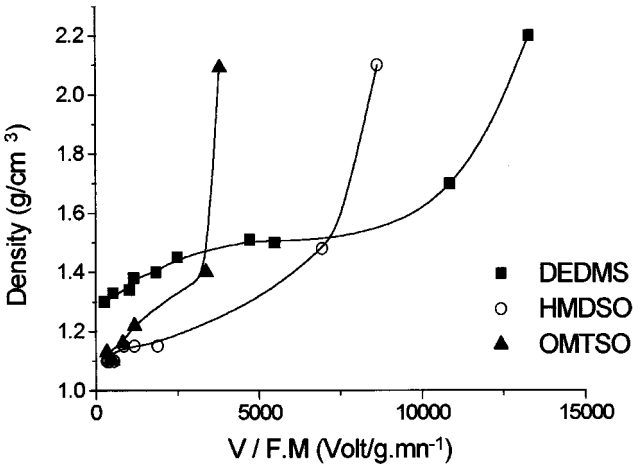

Figure 8. Films density vs. $V/F \cdot M$.

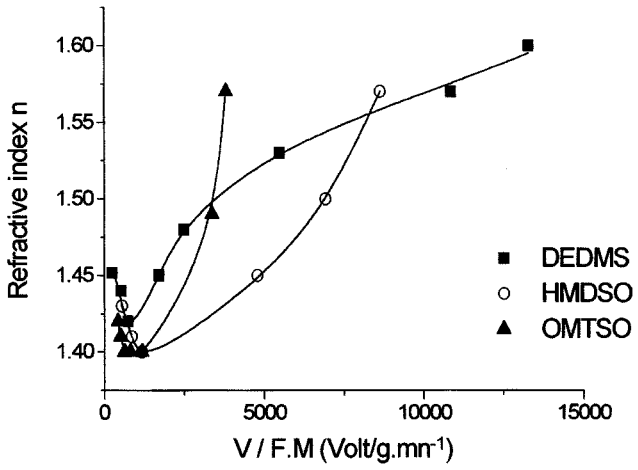

Figure 9. Films refractive index vs. $V/F \cdot M$.

produce films either composed mainly of silica or nearly silicone polymers, depending on whether the plasma conditions are hard or soft. This is in agreement with the results of Matsuyama (Matsuyama et al., 1994c).

Polymer-density determination

The evolution of the film density of different plasma polymers vs. the $V/F \cdot M$ parameter is presented in Figure 8. As $V/F \cdot M$ increases, we can see that the film density regularly rises from a minimum value of 1.25 g/cm^3 to 2.2 g/cm^3 (density value of SiO_2) for PP-DEDMS films, and from 1.15 to 2.1 g/cm^3 for PP-HMDSO and PP-OMTSO deposits. This is indicative of the extensive cross-linking and inorganic structural content already mentioned, due to a stronger fragmentation of monomer molecules when the plasma conditions become harder (Wrobel et al., 1980). Figure 8 also shows that the longer the monomer siloxane chain is, the sharper the variations in the density are in a narrower field of $V/F \cdot M$ values (reduction of the field toward the lowest $V/F \cdot M$ values).

Refractive index determination

The evolution of the films' refractive index for three different plasma polymers as a function of the $V/F \cdot M$ value is given in Figure 9. Except for the saturation region ($V/F \cdot M <$ 800 V/g$\cdot$min^{-1}), where the tendency is reversed, the refractive index n rises from 1.40–1.42 to 1.58–1.6 when $V/F \cdot M$ increases for the three monomers. This increase can be attributed, at least in part, to the extensive incorporation of carbon due to an easier redecomposition of hydrocarbon fragments when the plasma conditions become harder (Rau and Kulisch, 1994). The increase in n can also be explained by the previously seen increase in the film density (Lucovsky, 1987).

Permeation performances

All gas permeation experiments were performed on films deposited under nonsaturation plasma conditions. In order to investigate the influence of the nature of the porous substrate on the membranes' permeation properties, we deposited the same type of film (PP-DEDMS) on three different porous supports: mixed cellulosic esters, polypropylene, and alumina. The films were synthesized using identical plasma conditions (rf voltage = 50 V – monomer flow rate = 4.47×10^{-4} mol$\cdot$min^{-1} – total pressure = 0.4 mbar). The measured permeability coefficients using N_2, H_2, O_2, CO_2, and CH_4 are reported in Figure 10. We can observe that the porosity, mean pore size, and/or nature of the porous support don't have any influence on the membranes' permeability, which seems to be the result of just the gas transport through the plasma polymers. This result was expected because the resistance of porous substrates to gas transport is very low compared with that of dense films; indeed, the gas permeability of the three supports studied is very high (10^{-12} to 10^{-10} m$\cdot$mol$\cdot$m$^{-2}\cdot$s$^{-1}\cdot$Pa^{-1} order of magnitude). This result is very important because it means that this type of membrane can be successfully prepared in terms of pinhole-free layer and good thin-film adhesion on different kinds of substrates. Indeed, plasma parameters seem to be the most important factor in membrane manufacturing. The MF 25 support was chosen in order to continue our work, because it presents the necessary mechanical characteristics for manipulation without any special assistance.

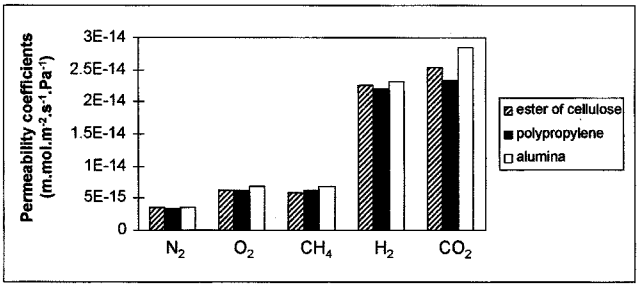

Figure 10. Permeability coefficients of PP-DEDMS films deposited on different porous substrates (rf voltage = 50 V; monomer flow rate = 4.47×10^{-4} mol$\cdot$min^{-1}; total pressure = 0.4 mbar).

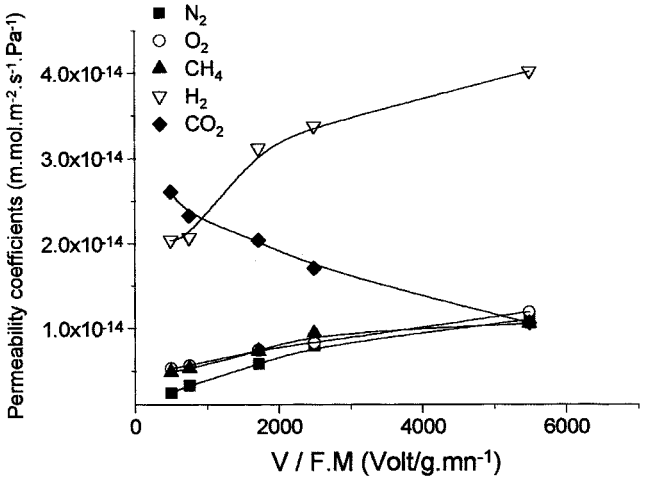

Figure 11. Gas permeability coefficients of PP-DEDMS films.

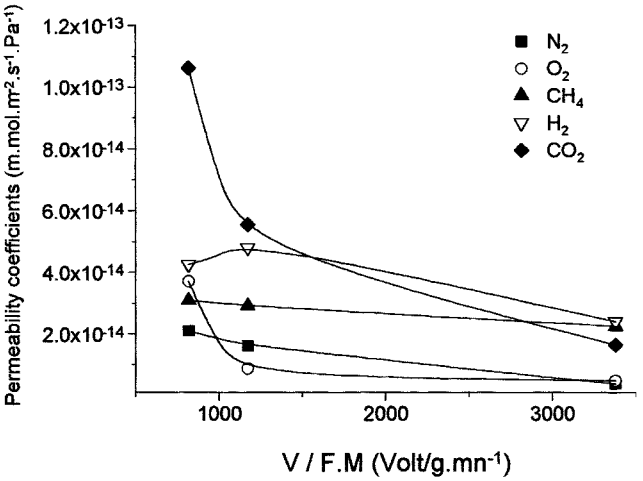

Figure 13. Gas permeability coefficients of PP-OMTSO films.

The gas permeability through silicone-type plasma membranes occurs via a solution-diffusion mechanism (Van Krevelen, 1976; Görbig, 1998). The molecular diffusion through the polymer matrix (microvoids) is a kinetic parameter related to the polymer-free volume and chain flexibility, whereas the solution coefficient is a thermodynamic parameter that depends directly on the gas–polymer interactions. The ideal selectivity and permeability changes observed macroscopically arise from the balance between both contributions. Obviously the behavior is different for each tested gas.

The influence of plasma parameters and the nature of the precursor on the membranes' permeation characteristics at various applied rf voltages (V) and precursor flow rates (F) was studied. The evolution of the gas permeability coefficients is represented as a function of the composite parameter $V/F \cdot M$ in Figures 11 to 13 for DEDMS, HMDSO, and OMTSO, respectively. In these three figures, we can see that, independent of the $V/F \cdot M$ value, and for all studied gases, the permeability coefficients are globally 10 to 40 times lower than those previously observed for the PDMS membranes reported in the literature (Stern, 1994; Stern et al., 1987); indeed, plasma polymers are much more highly cross-linked than are conventional polymers. In general, the highest permeability values are obtained for CO_2 (between 1.1×10^{-14} and 1.1×10^{-13} $m\cdot mol\cdot m^{-2}\cdot s^{-1}\cdot Pa^{-1}$, depending on the plasma conditions and the nature of the precursor) and H_2 (2.1×10^{-14}–4.8×10^{-14} $m\cdot mol\cdot m^{-2}\cdot s^{-1}\cdot Pa^{-1}$), which are known to be "rapid gases." This category includes migrants whose high molecular mobility through intermolecular voids is due to a low kinetic diameter, and gases that have a strong polar character, making them highly soluble in polymer films. H_2, which has the lowest kinetic diameter [2.89 Å (Shelekhin et al., 1992)], is the most mobile gas. CO_2 is also a small gas (kinetic diameter equal to 3.3 Å) that also has a strong polar character: for CO_2, the solubility coefficient is a very important parameter for the global mass transfer (Stern, 1994; Neel and Stern, 1990). On the other hand, O_2, N_2, and CH_4, which are rather large molecules (kinetic diameters equal to 3.46, 3.64, and 3.8 Å, respectively), without any dipolar moment, are "slow gases" (permeabilities between 2.4×10^{-15} and 4.3×10^{-14} $m\cdot mol\cdot m^{-2}\cdot s^{-1}\cdot Pa^{-1}$).

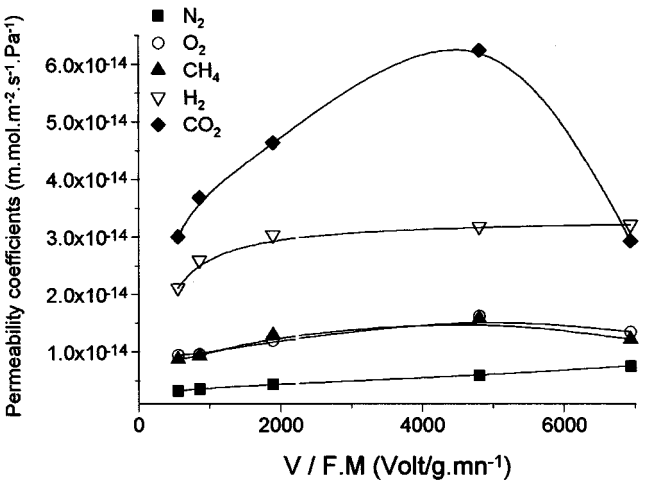

Figure 12. Gas permeability coefficients of PP-HMDSO films.

The variations in gas permeabilities displayed in Figures 11 to 13 depend on both the nature of the precursor and the $V/F \cdot M$ parameter, and are directly correlated with the changes in the physicochemical properties previously shown, in particular with the behavior of the "polymerization ratio" T represented in Figure 6. In the case of DEDMS and HMDSO (Figures 11 and 12), and for all gases except CO_2, we can see that the permeation performances of both types of membranes are similar in terms of the permeability value and changes with the $V/F \cdot M$ parameter. The permeability coefficients increase with the $V/F \cdot M$ value in spite of the density increase previously shown (Figure 8). This type of behavior has already been reported by Stern for PDMS membranes (Stern, 1994), and could be explained by the enhancement of the gas diffusivity due to the decrease in chain stiffness (that is, increase in the intrasegmental mobility). This results from the increase in the number of flexible siloxane bonds in relation to the rigid Si–C bonds: indeed the

[Si−CH_3]/[Si−O−Si or Si−O−C] ratio noted T decreases when $V/F\cdot M$ increases (Figure 6). This result is in good agreement with the fact that the highest permeability is observed for H_2, the smaller gas. At this point we could compare this type of membrane with the microporous ones where the mass transfer is realized through a molecular-sieve mechanism. Indeed the most important parameter of the gas transport of N_2, H_2, O_2, and CH_4 in PP-DEDMS and PP-HMDSO polymers seems to be the diffusivity, which is strongly related to the intermolecular voids and the ratios of the kinetic-gas diameters.

Because of its high solubility, the behavior of CO_2 is completely different from that of the other gases and varies according to the nature of the monomer. In terms of the values of CO_2 permeability, the PP-HMDSO films are much more permeable (between 2.9×10^{-14} and 6.3×10^{-14} $m\cdot mol\cdot m^{-2}\cdot s^{-1}\cdot Pa^{-1}$) than PP-DEDMS films ($1.1\times10^{-14}$–$2.6\times10^{-14}$ $m\cdot mol\cdot m^{-2}\cdot s^{-1}\cdot Pa^{-1}$). This result can be explained by the fact that polymers from HMDSO are much more organic and polymerized than are the films from DEDMS; in particular, PP-HMDSO films are characterized by higher T ratios than are PP-DEDMS films (Figure 6). In the case of PP-DEDMS films, the CO_2 permeability coefficient decreases with the $V/F\cdot M$ ratio. This change is directly related to the decrease in the organic character of the film as the plasma energy increases. For PP-DEDMS, the transport of CO_2 is mostly ensured by the contribution of the solubility coefficient: P (CO_2) decreases with $V/F\cdot M$ because CO_2 shows a greater affinity toward materials with a higher organic character. In the case of PP-HMDSO films, the evolution of P (CO_2) as a function of $V/F\cdot M$ is more atypical. Two regions can be distinguished: for $V/F\cdot M < 4{,}800$ $V\cdot min\cdot g^{-1}$, the diffusion parameter seems to be the limiting factor: the increase in chain flexibility (shown by the decrease in the [Si−CH_3]/[Si−O] ratio) causes the increase in $P(CO_2)$ with $V/F\cdot M$. In this region the behavior of CO_2 is similar to that of other gases. Beyond this limit, where $P(CO_2)$ reaches a maximum (6.3×10^{-14} $m\cdot mol\cdot m^{-2}\cdot s^{-1}\cdot Pa^{-1}$), the permeability coefficient decreases with $V/F\cdot M$: the solubility coefficient seems to become the limiting factor as the polymer evolves toward a silicalike material. It is interesting to see that, at the $V/F\cdot M =$ 4,800 $V\cdot min\cdot g^{-1}$ value corresponding to the $P(CO_2)$ maximum, both T curves related to DEDMS and HMDSO intersect (see Figure 6). Thus the change in the mass-transfer mechanism of CO_2 through PP-HMDSO can be related to a change in the chemical structure of these films caused by the T ratio passing above or below a critical value.

The case of PP-OMTSO is unique. In that case, these films present very high permeability coefficients for all gases (two to three times higher than permeabilities through PP-HMDSO and PP-DEDMS) because OMTSO has the longest siloxane chain (Figure 13). Indeed, the longer the monomer siloxane chain is, the more siloxane bonds are present in the polymer, and so the more flexible the resulting material is (Matsuyama, 1994a). Because of the high organic character (shown by the high T ratio) of PP-OMTSO at low $V/F\cdot M$ values, the mass transfer seems to be almost solely dependent on the solubility coefficient in the first part of the curves. Indeed, the permeability coefficients of N_2, H_2, and CH_4 are almost constant, whereas $P(CO_2)$ and $P(O_2)$ decrease steeply when the polymers tend to a more inorganic structure. The rapid decrease in $P(CO_2)$ and $P(O_2)$ with $V/F\cdot M$ is comparable to the sharp drop in the T ratio shown in Figure 6, and is related to the rather high kinetics of change toward a silicalike material. For high $V/F\cdot M$ ratios, PP-OMTSO films present permeabilities of the same order as those of PP-DEDMS and PP-HMDSO. This result indicates that all of the polymers studied evolve toward the same type of mineral material with the same T ratio (0) and density (2.2 g/cm^3) when $V/F\cdot M$ increases, even if the kinetics of change are different.

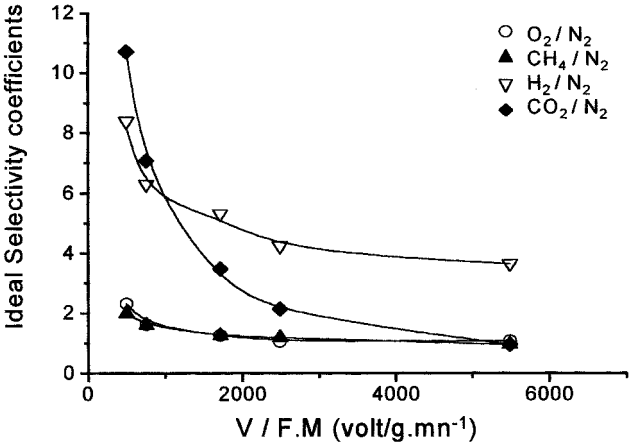

Figure 14. Ideal selectivity coefficients of PP-DEDMS films.

The differences in the ideal selectivity coefficients are given as a function of the composite parameter $V/F\cdot M$ for DEDMS, HMDSO, and OMTSO, respectively (Figures 14 to 16). Table 3 shows the ideal selectivities related to PDMS (Neel and Stern, 1990) and to Knudsen transport. In the case of DEDMS and HMDSO (Figures 14 and 15), at the lowest $V/F\cdot M$ value, our membranes show permselectivities that are at least equal to those of PDMS and that are even better for H_2/N_2 equal to 7–8. When $V/F\cdot M$ increases, the permselectivities $\alpha(H_2/N_2)$, $\alpha(O_2/N_2)$, and $\alpha(CH_4/N_2)$ logically decrease with the $V/F\cdot M$ ratio at the same time as the permeability increase already observed (Figures 11 and 12). The

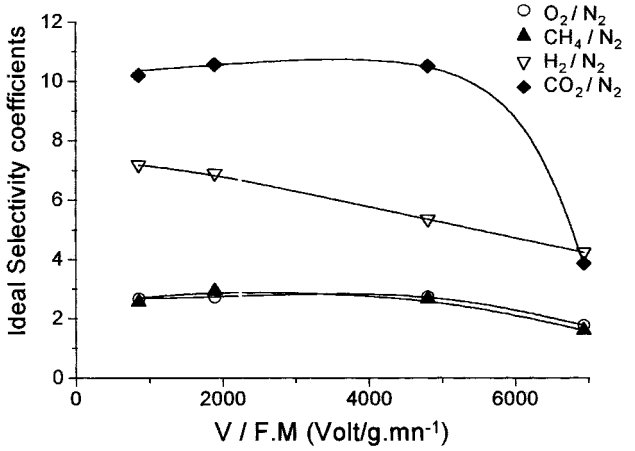

Figure 15. Ideal selectivity coefficients of PP-HMDSO films.

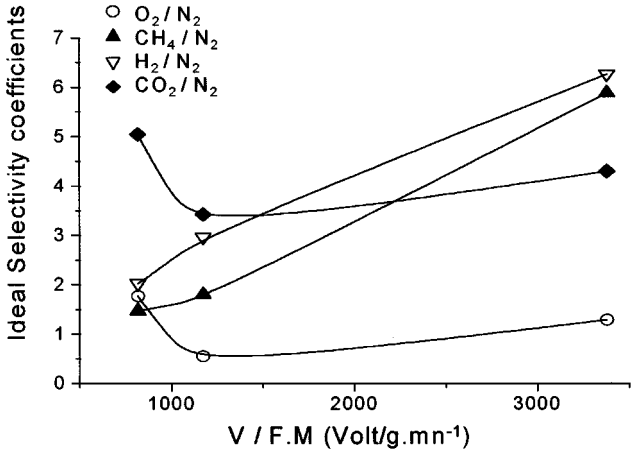

Figure 16. Ideal selectivity coefficients of PP-OMTSO films.

same trend can be observed for $\alpha(CO_2/N_2)$ in PP-DEDMS membranes: $\alpha(CO_2/N_2)$ decreases dramatically (from 11 to 1) as $V/F\cdot M$ increases, due to the reduction in the number of organic groups that strongly interact with CO_2 molecules. In the case of PP-HMDSO films, $\alpha(CO_2/N_2)$ remains maximum (equal to 10.5) for low $V/F\cdot M$, even if $P(CO_2)$ increases. This permselectivity is maintained as long as the diffusion contribution predominates ($V/F\cdot M < 4{,}800$ V·min·g^{-1}). As soon as the mass transfer is governed by the solubility coefficient ($V/F\cdot M > 4{,}800$ V·min·g^{-1}), $\alpha(CO_2/N_2)$ decreases sharply, as in PP-DEDMS membranes. In the hardest conditions, PP-DEDMS and PP-HMDSO films exhibit pure Knudsen selectivities due to the probable presence of defects in the most organic deposits (Weichart and Müller, 1993).

Much more permeable than the two other types of membranes, PP-OMTSO films synthesized under the softest plasma conditions are characterized by ideal selectivities at least two times lower than PP-DEDMS and PP-HMDSO (Figure 16). At low $V/F\cdot M$ values, where the solubility contribution is predominant, $\alpha(CO_2/N_2)$ and $\alpha(O_2/N_2)$ decrease as $V/F\cdot M$ increases, while $\alpha(H_2/N_2)$ and $\alpha(CH_4/N_2)$ increase. As fast as $V/F\cdot M$ increases further, all permselectivities then increase at the same time as the previously observed permeabilities decrease (Figure 13). This increase is above all marked for $\alpha(H_2/N_2)$ and $\alpha(CH_4/N_2)$, which is difficult to explain, because H_2 and CH_4, present very different kinetic diameters (2.89 Å and 3.8 Å, respectively) and molecular weights. At a high $V/F\cdot M$ value, all permselectivities with respect to N_2 are higher than the Knudsen ones. A comparison could be made with the results previously reported by Uhlhorn et al. (1992) for microporous silica membranes. We will continue this work with the study of diffusion coefficients (using a very precise permeametry apparatus) in order to better understand the observed results.

Table 3. Ideal gas Selectivity Coefficients Related to PDMS and Knudsen Transport

	H_2/N_2	CO_2/N_2	O_2/N_2	CH_4/N_2
PDMS (Néel and Stern, 1990)	2.31	11.5	2.14	3.39
Knudsen	3.74	0.8	0.94	1.32

Conclusion

We have shown that both the structural and the gas permeation properties of plasma-deposited films are correlated with the nature of the monomer, the monomer flow rate (F), and the rf voltage (V). An important parameter is the composite parameter $V/F\cdot M$, which is proportional to the factor of Yasuda W/FM, which characterizes the more or less energetic character of the plasma. At low $V/F\cdot M$ ratios, films have a density that is close to 1.2 g/cm^3 and get chemically close to polydimethylsiloxane polymer films. High $V/F\cdot M$ values lead to the formation of much denser films (density equal to 2.2 g/cm^3) compared to silicon dioxide polluted by carbon. At the same time, the gas permeation properties show characteristic changes. At low $V/F\cdot M$, PP-DEDMS and PP-HMDSO films, which are characterized by high $[Si-CH_3]/[Si-O-]$ ratios, show minimum permeabilities to all gases except to CO_2, which is very soluble in organic materials. Permselectivities are superior or equal to PDMS ones. With increasing $V/F\cdot M$, films are more mineral: the permeabilities of N_2, H_2, O_2, and CH_4 increase with the number of siloxane bonds. The evolution of $P(CO_2)$, which is more atypical, arises from the balance between increasing diffusivity and decreasing solubility. In PP-DEDMS, $P(CO_2)$ decreases because the limiting transfer factor is the solubility coefficient. This is also the case in PP-HMDSO at high $V/F\cdot M$; in the latter films, the trend is reversed at low $V/F\cdot M$, where the diffusion coefficient is the more important transport factor. Because of the long siloxane chain of OMTSO, PP-OMTSO layers exhibit the highest permeabilities and lowest permselectivities. The rapid change in these films toward a silicalike material causes an increase in all ideal gases' separation factors with respect to N_2 at high $V/F\cdot M$. In a future work, we will report the determination of the diffusion coefficients and the modeling of the relation between the gas transport properties and the structural parameters.

Literature Cited

Anderson, D. R., "Infrared, Raman and Ultraviolet Spectroscopy," *Analysis of Silicones*, A. L. Smith, ed., Wiley-Interscience, New York, p. 247 (1974).

Bell, A. T., "Fundamentals of Plasma Chemistry," *Techniques and Applications of Plasma Chemistry*, J. R. Hollan and A. T. Bell, eds., Wiley, New York (1974).

Catherine, Y., and A. Zamouche, "Glow Discharge Deposition of Tetramethylsilane Films," *Plasma Chem. Plasma Process.*, **5**, 353 (1985).

Chapman, B., *Glow Discharge Processes—Sputtering and Plasma Etching*, Wiley, New York, p. 149 (1980).

D'Agostino, R., *Plasma Deposition, Treatment, and Etching of Polymers*, Academic Press, San Diego (1990).

Görbig, O., S. Nehlsen, and J. Müller, "Hydrophobic Properties of Plasma Polymerized Thin Film Gas Selective Membranes," *J. Membr. Sci.*, **138**, 115 (1998).

Inagaki, N., "Gas Selective Plasma Polymerization Membrane," *Mol. Cryst. Liq. Cryst.*, **224**, 123 (1993).

Inagaki, N., *Plasma Modification and Plasma Polymerization*, Technomic, Lancaster (1996).

Lee, S. H., and D. C. Lee, "Preparation and Characterization of Thin Films by Plasma Polymerization of Hexamethyldisiloxane," *Thin Solid Films*, **325**, 83 (1998).

Lucovsky, G., M. J. Manitini, J. K. Srivastava, and E. A. Irene, "Low-Temperature Growth of Silicon Dioxide Films: A Study of Chemical Bonding by Ellipsometry and Infrared Spectroscopy," *J. Vac. Sci. Technol. B*, **5**, 530 (1987).

Matsuyama, H., A. Kariya, and M. Teramoto, "Effect of Siloxane Chain Lengths of Monomers on Characteristics of Pervaporation Membranes Prepared by Plasma Polymerization," *J. Appl. Poly. Sci*., **51**, 689 (1994a).

Matsuyama, H., T. Shiraishi, and M. Teramoto, "Plasma Polymerized Membranes from Organosilicon Compounds for Separation of Oxygen over Nitrogen," *J. Appl. Poly. Sci*., **54**, 1665 (1994b).

Matsuyama, H., A. Kariya, and M. Teramoto, "Characteristics of Plasma Polymerized Membrane from Octamethyltrisiloxane and Its Application to the Pervaporation of Ethanol-Water Mixture," *J. Memb. Sci*., **88**, 85 (1994c).

Néel, J., and S. A. Stern, "Le Fractionnement des Mélanges Gazeux par Perméation. Etat Actuel du Développement du Procéde," *ENTROPIE*, **157–158**, 35 (1990).

Parrat, L. G., "Surface Studies of Solids by Total Reflection of X-Rays," *Phys. Rev*., **95**, 359 (1954).

Rau, C., and W. Kulisch, "Mechanisms of Plasma Polymerization of Various Silico-Organic Monomers," *Thin Solid Film*, **249**, 28 (1994).

Roualdes, S., M. Theobald, J. Sanchez, and J. Durand, "Gas Separation with Organosilicon Plasma Polymers Deposited on Porous Substrates," *Proc. Int. Conf. on Inorganic Membranes*, Nagoya, Japan (1998).

Shelekhin, A. B., A. G. Dixon, and Y. H. Ma, "Adsorption, Permeation and Diffusion of Gases in Microporous Membranes: II. Permeation of Gases in Microporous Glass Membranes," *J. Memb. Sci*., **75**, 233 (1992).

Smith, A. L., *Applied Infrared Spectrocopy*, Wiley, New York, p. 286 (1977).

Stern, S. A., "Polymers for Gas Separation: The Next Decade," *J. Memb. Sci*., **94**, 1 (1994).

Stern, S. A., V. M. Shah, and B. J. Hardy, "Structure Permeability Relationships in Silicone Polymers," *J. Poly. Sci. Part B: Poly. Phys.*, **25**, 1263 (1987).

Uhlhorn, R. J. R., K. Keizer, and A. J. Burggraaf, "Gas Transport Separation with Ceramic Membranes: II. Synthesis and Separation Properties of Microporous Membranes," *J. Memb. Sci*., **66**, 271 (1992).

Van Krevelen, D. W., and P. J. Hofyzer, *Properties of Polymers*, Elsevier, Amsterdam (1976).

Wagner, C. D., W. M. Riggs, L. E. Davis, and J. F. Moulder, *Handbook of X-Ray Photoelectron Spectroscopy*, G. E. Mullenberg, ed., Perkin-Elmer, Physical Electronics Division, Eden Prairie, MN (1978).

Weichart, J., and J. Müller, "Plasma Polymerization of Silicon Organic Membranes for Gas Separation," *Surf. Coating Technol*., **59**, 342 (1993).

Wrobel, A. M., M. R. Wertheimer, J. Dib, and H. P. Schreiber, "Polymerization of Organosilicones in Microwave Discharges," *J. Macromol. Sci.-Chem. A*, **14**, 321 (1980).

Yasuda, H., "Glow Discharge Polymerization," *Thin Film Processes*, J. Vossen and W. Kern, eds., Academic Press, New York, p. 361 (1978).

Manuscript received Dec. 31, 1998, and revision received Apr. 2, 1999.